instruments

MDPI

Article

Luminescence Response and Quenching Models for Heavy Ions of 0.5 keV to 1 GeV/n in Liquid Argon and Xenon

Akira Hitachi

Waseda Research Institute for Science and Engineering, Shinjuku, Tokyo 169-8555, Japan; a.hitchi@kurenai.waseda.jp

Abstract: Biexcitonic collision kinetics with prescribed diffusion in the ion track core have been applied for scintillation response due to heavy ions in liquid argon. The quenching factors $q = E_L/E$, where E is the ion energy and E_L is the energy expended for luminescence, for 33.5 MeV/n ^{18}O and 31.9 MeV/n ^{36}Ar ions in liquid Ar at zero field are found to be 0.73 and 0.46, compared with measured values of 0.59 and 0.46, respectively. The quenching model is also applied for 80–200 keV Pb recoils in α-decay, background candidates in direct dark matter searches, in liquid argon. Values obtained are ~0.09. A particular feature of Birks' law has been found and exploited in evaluating the electronic quenching factor q_{el} in liquid Xe. The total quenching factors q_T for 0.5–20 keV Xe recoils needed for weakly interacting massive particle (WIMP) searches are estimated to be ~0.12–0.14, and those for Pb recoils of 103 and 169 keV are 0.08 and 0.09, respectively. In the calculation, the nuclear quenching factor $q_{nc} = E_\eta/E$, where E_η is the energy available for the electronic excitation, is obtained by Lindhard theory and a semi-empirical theory by Ling and Knipp. The electronic linear energy transfer plays a key role.

Keywords: WIMPs; CEνNS; Birks' law; scintillation quenching; liquid argon; liquid xenon; dark matter; recoil ions in α-decay; LET

Citation: Hitachi, A. Luminescence Response and Quenching Models for Heavy Ions of 0.5 keV to 1 GeV/n in Liquid Argon and Xenon. *Instruments* **2021**, *5*, 5. https://doi.org/10.3390/instruments5010005

Received: 27 November 2020
Accepted: 30 December 2020
Published: 11 January 2021

1. Introduction

Noble liquids are used in various fields of study in particle physics, high energy physics, cosmology and medicine. Noble liquids can be used for various types of detectors, including ionization chambers, scintillation detectors, proportional counters, proportional scintillation counters, photoionization detectors (PIDs), γ-cameras, positron emission tomography (PET), calorimeters and time projection chambers (TPCs) [1–4]. Noble liquids make ideal detector material because of high density and high Z (Xe), as well as high stopping power for γ-rays and β-rays, providing self-shielding from external backgrounds. Noble liquids have high electron mobility and no size limits, and they suffer no permanent radiation damage. A purification method capable of ~1 ppb (O_2 equivalent) has been established [4]. Although scintillation is in the vacuum ultraviolet (VUV) region, various wavelength shifters are available, and a VUV sensitive photomultiplier tube (PMT) with a high quantum efficiency, as high as 34%, has been developed for liquid Xe (LXe) [5].

Direct dark matter searches look for the slow recoil ions produced by elastic collisions with weakly interacting massive particles (WIMPs), the prime dark matter candidates. A massive noble-liquid detector can be a most powerful tool for dark matter searches. Two-phase TPCs using liquid Ar (LAr) or LXe have been constructed [4,6–8]. Footprints due to a few to tens of keV recoil ions are looked for. It is also extremely important to know the scintillation and ionization response to consider the possibility of detecting coherent elastic neutrino-nucleus scattering (CEνNS) with LAr and LXe. The technology needed for investigating CEνNS is similar to that for WIMPs; however, the required energy threshold is even lower, in keV or sub-keV [2,9–11].

A number of studies have investigated the scintillation response of noble-liquid detectors for light particles. However, investigations on scintillation quenching in high

linear energy transfer (LET; $-\mathrm{d}E/\mathrm{d}x$) are quite limited; they have considered α-particles, fission fragments (FFs) and relativistic heavy ions (RHI) of energy ~1 GeV/n [12] apart from slow recoils mentioned above. The information in the intermediate energy range of about 20–100 MeV/n is needed for studying high energy physics and nuclear physics as well as for studies on cosmic ray heavy ions as a radiation hazard in manned space flights. LAr and LXe are some of the strongest scintillators against scintillation quenching at high LET. Both the ionization and the scintillation signals can be used, and a combination of the two signals gives many advantages. Scintillation and ionization studies on ^{18}O and ^{36}Ar ions of ~30 MeV/n in liquid Ar with and without allene doping were performed, and an energy resolution of 0.37% FWHM was achieved with 80 ppm allene [13,14]. The biexcitonic collision kinetic theory is the only theory that works in wide ranges of LET and ion velocity [15]. The previous results provide a reasonable fit to the overall trend of the experimental data in LAr with reasonable specific reaction rates given by a dipole–dipole collision cross-section ~2.5 Å^2 to a quarter hard-sphere collision cross-section 43 Å^2. The theory is still worth investigating and can be refined. The experimental results for ^{18}O and ^{36}Ar ions of ~30 MeV/n provide information on scintillation response in this energy region.

It is important to create well-defined models for the response of detector media. Because of its simple structure and known electronic states where the emission originates from, noble liquids are suitable materials with which to study luminescence response to various ions. In this paper, the exciton–exciton collision diffusion kinetics is applied for the scintillation efficiency (quenching factor) for ~30 MeV/n O and Ar ions and 80–200 keV Pb recoils in LAr. The collision theory is not ready for LXe. The theory is compared with Birks' law, and a particular feature of Birks' law is revealed. This feature of Birks' law is exploited and applied for obtaining quenching factors for 0.5–20 keV Xe recoils and 103 and 169 keV Pb recoils in LXe. No theoretical studies have been previously made for quenching factors for Pb recoils in LAr and LXe. We refer to noble liquid as liquid Ar and Xe unless otherwise mentioned.

2. Materials and Methods

Numbers of excitons and electron–ion pairs are produced in noble liquids when excited by charged particles. Ionizations and excitations go to free exciton states R*, then self-trapped R_2*. Luminescence is due to the transition from the lowest excimers, $^1\Sigma_u^+$ and $^3\Sigma_u^+$, to the repulsive ground state $^1\Sigma_g^+$ [16]:

$$R_2^* \rightarrow R + R + h\nu \quad (1)$$

a broad structureless emission centered at 128 and 175 nm, respectively, in LAr and LXe. There are no nonradiative passes to the ground state. The lifetimes of the excimer do not depend on whether quenching occurs or not, though the singlet to triplet intensity ratio I_S/I_T changes [17]. Therefore, the excimers are excluded from the candidate responsible for quenching. The "free" excitons are Wannier excitons, Γ(1/2) and Γ(3/2), which may be treated as rapidly moving particles with the mass m* close to the electron mass m_e. In spite of their very short lifetimes (~1 ps), these excitons play important roles in collisional energy transfers such as Penning ionization [16]. Exciton–exciton collision is proposed for luminescence quenching [15,17]:

$$R^* + R^* \rightarrow R + R^+ + e^- (\text{kinetic energy}) \quad (2)$$

The ejected electron losses its kinetic energy before recombination. Only one excitation, i.e., one VUV photon, remains after recombination.

An analysis of the scintillation quenching from first principles is not possible for most scintillators because of the complex nature of the scintillation process. Birks' law is widely

used in organic scintillators, with considerable success [18,19]. The specific fluorescence, dL/dr, is expressed as a function of the specific energy loss, dE/dr:

$$\frac{dL}{dr} = \frac{AdE/dr}{1 + k_B B dE/dr} \tag{3}$$

where r is the residual range, $r = R - x$ and $dr = -dx$ (R: the range). A and $k_B B$ are treated as fitted constants. Birks' law was originally proposed for quenching mechanism via capture of an excited state by a transient damaged molecule in a cylindrical ion track in organic scintillators [18]. Birks' law is often expressed as the following form for practical uses, dividing both sides of Equation (3) by dE/dr:

$$\frac{dL}{dE} = \frac{A}{1 + k_B B dE/dr} \tag{4}$$

The scintillation yield, or the quenching factor q, is expressed as a function of LET ($= -dE/dx$). Birks' law is also applied for inorganic crystals at a high LET region. However, the scintillation is not a simple function of LET in noble liquids, as shown in Figure 1a. q depends on the velocity v, or energy in MeV/n, and also on the track structure. Birks' law has an implicit assumption that the radius of the cylindrical ion track is constant, as discussed in Appendix A.

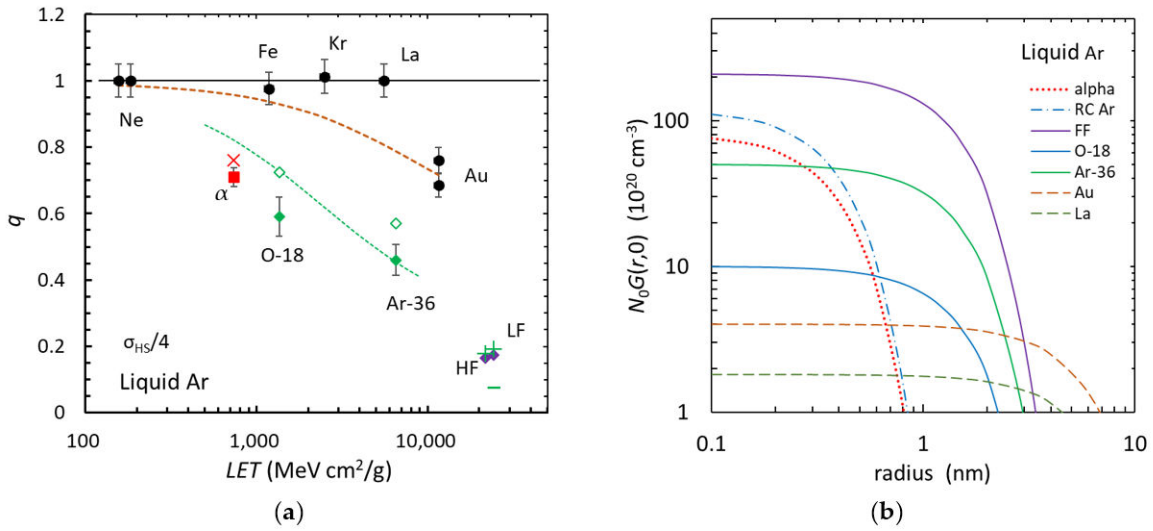

Figure 1. (**a**) Quenching factor q for various ions as a function of linear energy transfer (LET) in liquid Ar. Measurements are as follows: 5.305 MeV ^{210}Po α-particles (•), relativistic heavy ions (RHIs) of ~1 GeV/n (•) [12], 33.5 MeV/n ^{18}O and 31.9 MeV/n ^{36}Ar ions (closed diamonds) [14] and ^{252}Cf fission fragments (closed diamonds) [12]. Heavy fragments (HFs) and light fragments (LFs) are shown separately. Crosses (×,+) show the results calculated numerically for the hard-sphere cross-section divided by 4, $\sigma_{HS}/4$. The previous result obtained for LFs with $T_c/T = 1$ is also shown (-). Dashed curves show Birks' law applied to the numerical calculation for core quenching (Equation (27)) as shown in Figure 3b. RHIs and nonrelativistic ions (^{18}O, ^{36}Ar and FFs) are treated separately. Open diamonds show q obtained by the sum of scintillation and charge signals [14] (see Section 4.3). (**b**) Initial radial distribution of excited species, essentially the same as the prompt dose profile, in the cylindrical track core produced by various ions in liquid Ar (see Section 2.1). The distribution for 30 keV Ar recoils (RC Ar) is also shown (dot-dashed curve). A Gaussian distribution is assumed.

2.1. Track Structure

The heavy-ion track structure consists of a cylindrical core surrounded by a penumbra [20,21]. The core is mainly generated by continuous excitation and ionization by the primary ion in glancing (distant) collisions. Some of the secondary electrons, δ-rays, produced by knock-on (close) collisions, deposit their energy outside, forming the penumbra. The δ-rays deposit a part of their energy in the core. The LET of δ-rays is about one order

of magnitude less than that of the primary ion. We assume that quenching occurs in the high-excitation density core. The energy of the incident ions T is divided into the core T_c and the penumbra T_p. The energy available for scintillation T_s is [15]

$$T_s = qT = q_c T_c + T_p \tag{5}$$

where q_c is the quenching factor in the core and q is the overall quenching factor, defined as $q = 0$ for the total quenching and $q = 1$ for no quenching. Typical stopping theories such as Bethe and Lindhard [22] tell the equipartition rule, stating equality of stopping contributions from glancing collisions and close collisions. The core radius a_0 for nonrelativistic ions is given by the Bohr criterion:

$$r_B = \hbar v / 2E_1 \tag{6}$$

where $\hbar$ is Planck's constant divided by 2π, v is the incident ion velocity and E_1 is the energy of the lowest excited state of the medium, 12.1 and 8.2 eV for LAr and LXe, respectively [16]. For relativistic particles, the density effect becomes important and Fermi's theory is used. The core radius is given by

$$r_0 = \lambda\beta \tag{7}$$

where λ is the maximum core size; λ = 6.78 nm in LAr [15]. The fractional energy deposited in the core (T_c/T) for O ions of 33.5 MeV/n (β = 0.261) and Ar ions of 31.9 MeV/n (β = 0.255) was set 0.75, taken from the previous calculations for protons of 17.8 and 38.2 MeV [15]. Ions of ~30 MeV/n should be considered nonrelativistic, and the Bohr criterion was taken. We took a modified core and penumbra track structure, a Gaussian distribution of dose in the core. The initial distribution of excited species in the track core produced by various ions in LAr is shown in Figure 1b.

2.2. Biexcitonic Collision Kinetics

The density distribution of the track structure is not sufficient to obtain scintillation efficiency, as shown in Figure 1b. The quenching factors measured for α-particles and relativistic Au ions are close to each other (Figure 1a), whereas the density of the excited species at the core axis for α-particles is about 20 times that for Au ions (Figure 1b). Some reaction kinetics are needed. This model includes an evaluation of the initial dose profile with consideration of the track structure, the diffusion of excitons and a second-order reaction process with an evaluated specific rate. The exciton motion is treated as coherent in the evaluation of the rate. The details of the calculation have been described in [15] and, therefore, are only briefly discussed here. No self-absorption and no nonradiative transitions from the self-trapped exciton states to the ground state exist in noble liquids. The diffusion-kinetic equations for free (suffix 1) and the self-trapped (suffix 2) excitons may be expressed as

$$\partial n_1/\partial t = D\nabla^2 n_1 - n_1/\tau - k n_1^2 \tag{8}$$

and

$$\partial n_2/\partial t = n_1/\tau - A_2 n_2 \tag{9}$$

where n is the exciton density, D is the diffusion coefficient of the free exciton, k is the specific rate of biexcitonic quenching and τ is the free exciton lifetime against self-trapping. A_2 is the radiative decay constant for self-trapped excitons. In cylindrical geometry we write with Gaussian approximation:

$$n_1(r,t) = N(t)G(r,t) \tag{10}$$

where $N(t)$ is the number of free excitons per unit length and $G(r,t)$ is a normalized Gaussian distribution; $G(r,t) = (\pi {a_t}^2)^{-1}\exp(-r^2/{a_t}^2)$ with ${a_t}^2 = {a_0}^2 + 4Dt$. Under standard boundary condition, Equation (8), integrating over all r, we obtain

$$\frac{\mathrm{d}N}{\mathrm{d}t} = -\frac{N}{\tau}kN^2\int_0^\infty G^2(2\pi)\mathrm{d}r \tag{11}$$

solved in the usual manner. The result is given as

$$N(t) = N_0\mathrm{e}^{-t/\tau}\left[1 + \frac{kN_0}{2\pi}\cdot\frac{\exp(a_0^2/4D\tau)}{4D}\{\mathrm{E}_1(u_0) - \mathrm{E}_1(u_t)\}\right]^{-1} \tag{12}$$

where N_0 is the initial number of free excitons per unit length and $\mathrm{E}_1(\xi)$ is the exponential integral

$$\mathrm{E}_1(\xi) = \int_\xi^\infty \frac{\mathrm{e}^{-\xi}}{\xi}\mathrm{d}\xi, \text{ and } u_0 = \frac{a_0^2}{4D\tau},\ u_t = \frac{a_0^2 + 4Dt}{4D\tau}. \tag{13}$$

Equation (12) shows the free exciton decay. Since $1/\tau >> A_2$, the population of self-trapped exciton per unit length N_2 is expressed as

$$\frac{\mathrm{d}N_2(t)}{\mathrm{d}t} = \frac{N(t)}{\tau} \tag{14}$$

The fraction q_c which survives biexcitonic collisions is obtained as:

$$q_c = N_2(\infty)/N_0 = \frac{\int_0^\infty (N(t)/\tau)\,\mathrm{d}t}{N_0} \tag{15}$$

We have calculated the number of self-trapped excitons up to $t/\tau = 4$.

The following approximation relates Birks' law to a solution of the second-order reaction kinetics adopted here as discussed in Appendix A. A normalized form is:

$$\frac{\mathrm{d}L}{\mathrm{d}E} = \frac{1}{1 + k\cdot\left[\frac{\exp(u_0)}{8\pi D}\mathrm{E}_1(u_0)\right]\cdot B\frac{\mathrm{d}E}{\mathrm{d}r}} \tag{16}$$

where $k_B = k\cdot[\ ]$ when a_0 can be regarded as constant.

2.3. Recoil Ions for Dark Matter Searches

The quenching model is also applied for slow recoil ions in dark matter searches and expected scintillation signals are discussed. Slow means $v << v_0$, where $v_0 = c/137$ is the Bohr velocity and c is the velocity of light. The total stopping power S_T for slow ions is the sum of the electronic stopping power S_e and the nuclear stopping power S_n: $S_T = S_e + S_n$ [23]. Lindhard et al. introduced dimensionless measures of energy ε and range ρ. One equation for the stopping power can be applied to collisions between any ion of Z_1 and M_1 and target atom of Z_2 and M_2, where Z and M are the atomic number and mass number, respectively, and suffixes 1 and 2 represent the projectile and the target atom, respectively. In dimensionless units, the electronic stopping power is expressed as $(\mathrm{d}\varepsilon/\mathrm{d}\rho)_e \cong \kappa\varepsilon^{1/2}$, where a constant κ is given by Z_1, Z_2, M_1 and M_2. A secondary nucleus can give some energy to electrons. After the collision cascades, the energy ε of the ion is given to the electronic excitation and nuclear motion. Only the energy η given to electronic excitation is available for scintillation and ionization. Lindhard et al. gave η values for κ = 0.10, 0.15 and 0.20 [23] (pp. 25–27). The nuclear quenching factor (Lindhard factor), $q_{nc} = \eta/\varepsilon$, was obtained by interpolation for κ = 0.165 for Xe recoil in Xe:

$$\eta = 0.4167\varepsilon^{1.149},\ \varepsilon\ <\ 0.05. \tag{17}$$

Dimensionless energies, ε and η, are converted to E and E_η, respectively, as $\varepsilon = 0.00104\ E$ (keV) and $\eta = 0.00104\ E_\eta$ (keV) and $q_{nc} = \eta/\varepsilon = E_\eta/E$. Analytic expressions for low energy stopping powers, S_e and S_n, based on the Lindhard theory, are given by Lindhard et al. [23] and by Biersack [24], respectively. The electronic LET (LET_{el}), the specific electronic energy loss, is defined as [25,26]

$$LET_{el} = -\frac{dE_\eta}{dx} = -\frac{dE_\eta}{dE}\cdot\frac{dE}{dx} = \frac{dE_\eta}{dE}\cdot S_T \tag{18}$$

Then, LET_{el} can be obtained analytically. The averaged LET_{el} for Xe recoil was taken as

$$LET_{el} = \int_0^E dE'(dE'_\eta/dE')\cdot S_T / \int_0^E dE' \tag{19}$$

The total quenching factor q_T is given as $q_T = q_{el}\cdot q_{nc}$ when average values are taken.

2.4. Heavy Recoil Ions in α-Decay

Heavy ions in α-decay may produce signals similar to those expected for WIMP collisions. It is critical for dark matter searches to achieve a very low background rate. The backgrounds are mostly due to light particles. However, Rn produces decay sequence and emits α-particles. A heavy ion, such as Po, Pb and Bi, is recoiled in α-decay. The recoiled nucleus does not make a background for dark matter searches because it is always associated with α-particles and easily rejected. However, if the α-decay occurs at the detector wall or the electrodes such that the α-particle goes into the wall and the Pb nucleus recoils into the active area it can make a serious background [26].

Stopping powers for Pb ions in Ar and Xe are shown in Figure 2. The evaluation of q_{nc} for $Z_1 \neq Z_2$ is quite hard. The recoil ions in α-decay in noble gases give one of the simplest cases. The α-decay produces a heavy ion with energy of 100–200 keV. The ionization measurements in gas basically provide the Lindhard factor q_{nc} both in gas and condensed phases. The factor q_{nc} is given by the W_α/W_{NR} ratio, where W_α and W_{NR} are W-values, the average energy expended to produce an electron–ion pair, for α-particles and nuclear recoils, respectively. Madsen [27] measured the ionization by recoil ions in α-decay from ^{210}Po, ThC (^{212}Bi) and ThC′ (^{212}Po). ^{210}Po gives 103 keV ^{206}Pb, ^{212}Bi gives 116 keV ^{208}Tl and ^{212}Po gives 169 keV ^{208}Pb. Jesse and Sadauskis [28] and Cano [29] also reported values close to that by Madsen for 103 keV ^{206}Pb recoils.

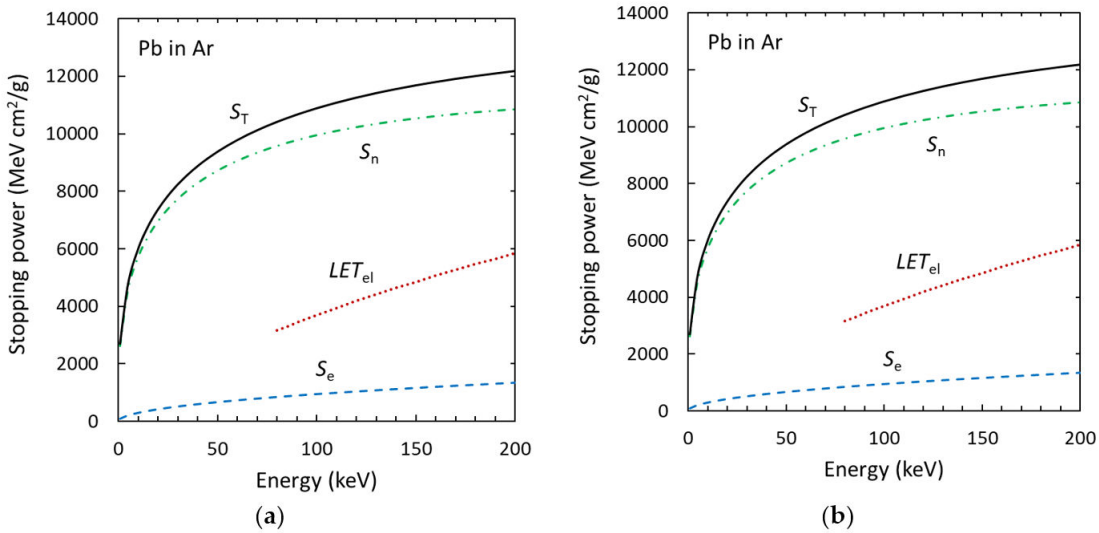

Figure 2. The stopping powers and the electronic LET for Pb ions: (**a**) in argon; (**b**) in xenon. LET_{el} was obtained by using a semi-empirical power-law approximation for q_{nc}.

Lindhard et al. [23] (pp. 33–41) obtained a power-law approximation for very low energy. Two characteristic energies, $E_{1c} \cong M_1{}^3(M_1{+}M_2)^{-2}Z^{4/3}Z_1{}^{-3}{\cdot}500$ eV and $E_{2c} \cong (M_1 + M_2)^2 M_1{}^{-1}\, Z_2{\cdot}125$ eV, where $Z^{2/3} = Z_1{}^{2/3} + Z_2{}^{2/3}$, set the upper boundary. We have

$$E_\eta = C_A E^{3/2} \text{ for } E \ll E_{1c},\ E_{2c} \tag{20}$$

where $C_A = \frac{2}{3}\{E_{1c}{}^{-1/2} + \frac{1}{2}\gamma^{1/2}E_c{}^{-1/2}\}$, $E_c = \gamma E_{2c}$ and $\gamma = 4M_1\, M_2\, /(M_1 + M_2)^2$. The straggling Ω^2 in E_η is also given. The relative straggling becomes constant with the same low energy approximation and given by

$$\Omega^2/E_\eta{}^2 = \frac{1}{14}\gamma\left\{\left(\frac{\gamma^{1/2}}{C_A E_c^{1/2}} - \frac{7}{4}\right) + \frac{7}{16}\right\} \tag{21}$$

The heavy recoil nuclei have practically the same atomic number and are treated here as Pb. The power-law approximations given for Pb ions are

$$E_\eta = 0.0192E^{3/2},\ \Omega^2/E_\eta{}^2 = 0.020 \text{ for } E < E2_c = 665 \text{ keV in Ar} \tag{22}$$

and

$$E_\eta = 0.0122E^{3/2},\ \Omega^2/E_\eta{}^2 = 0.041 \text{ for } E < 3.7 \text{ MeV in Xe} \tag{23}$$

The power-law approximation has been applied to obtain a Bragg-like curve, the energy deposition as a function of the projected range, for recoil ions in binary gases [26]. The curve is intended for directional searches for WIMPs in the gas TPC.

Ling and Knipp [30] presented an approximate equation for q_{nc} for a heavy particle ($Z = 82$, $M = 208$) in Ar. For $v/v_0 \ll 1$,

$$q_{nc} = E_\eta/E \approx \left[\frac{2}{3}a' + (16a''\gamma''/21)\right]v,\ v/v_0 \ll 1,\ E > 78 \text{ keV} \tag{24}$$

where $\gamma'' = 2M_1\ /\ (M_1 + M_2)$ and a', a'' are constants. They found that the measurement by Madsen [27] is well represented by the following equation:

$$q_{\mathrm{nc}} = \frac{W_\alpha}{(15.4 \text{ eV})}\frac{v}{v_0} \tag{25}$$

where $W_\alpha = 25$ eV in Ar + 5% air. Equation (25) can be expressed in the form of Equation (20) with $C_A = 0.0226$. The contribution of S_n dominates; the contributions to S_T are 91% and 9% by S_n and S_e, respectively, for 103 keV Pb recoils in argon. LET_el for Pb recoils is as large as $S_\mathrm{T}/3$ in argon as shown in Figure 2a.

Following Ling and Knipp [30], we use the W_α/W_NR ratio, $(22.0 \pm 0.3)/(158.8 \pm 8) = 0.139$, for 103 keV Pb recoils in Xe measured by Cano [29], and a semi-empirical power-law approximation may be written as

$$q_{\mathrm{nc}} = \frac{W_\alpha}{(22.5 \text{ eV})}\frac{v}{v_0} \tag{26}$$

where $W_\alpha = 22.0$ eV in Xe. We have Equation (20) with $C_A = 0.0137$.

Electronic quenching q_el in LAr is evaluated by Equation (15). A simple average $LET_\mathrm{el} = E_\eta/R$ is taken for Pb recoils. The averaged values are taken for q_nc and q_el, then the total quenching factor is given as $q_T = E_\mathrm{L}/E = q_\mathrm{nc}{\cdot}q_\mathrm{el}$.

3. Results

The diffusion-reaction model described here was applied before for α-particles, fission fragments and relativistic heavy ions [15]. Fairly good agreements with experimental data were obtained. The cross-sections for biexcitonic collisions used were within an acceptable range; however, this was a rather wide range, due to the dipole–dipole interaction of

σ_{dd} = 2.5 A^2 to a quarter hard-sphere cross-section, $\sigma_{HS}/4$ = 43 A^2. The dipole–dipole interaction and the exchange interaction are typical interaction mechanisms for atom–molecule collisions in thermal energy. The dipole–dipole interaction is applied for a process due to optically allowed transitions and is of a long range. The exchange interaction is applied for a process that includes the metastable states and is of a short range. Watanabe and Katsuura [31] gave a theoretical formula to obtain the cross-section σ_{dd} estimated from the transient dipole moment given by the photoabsorption coefficient. It is difficult to obtain the cross-sections σ_{ex} due to exchange interaction. Therefore, the hard-sphere cross-section σ_{HS} is often used as a measure of an upper limit of σ_{ex}. The magnitude for σ_{dd} is much larger than that for σ_{HS} for usual collisions in gas phase at room temperature. The exciton is treated as a free particle moving with the thermal velocity with a mass close to the electron mass, and a coherent motion model (like that in gas phase) is used. However, σ_{dd} is too small, partly because of the rapid free exciton motion. A typical thermal velocity of collision partners is ~5 × 10^4 cm/s at room temperature, and that for exciton–exciton collisions in LAr is ~1 × 10^7 cm/s at liquid argon temperature. We took $\sigma_{HS}/4$ in the present calculation. The energy transfer processes in solutions and ordinary solids such as organic crystals are discussed, e.g., in [32]. The numerical calculation for exciton–exciton reaction rate equations was performed for ^{18}O, ^{36}Ar ions and Pb recoils in α-decay in LAr. The results for FFs were reinvestigated. The constants needed for the quenching calculation were set the same as in the previous calculation [15]. These are as follows: τ = 1 ps, D = 1 cm^2/s, $k = \sigma v_{th}$, where v_{th} is the thermal velocity of collision partners, free excitons (v_{th} ~ 1.2 × 10^7 cm/s, μ* = 0.5 m_e, where μ^* is the effective reduced mass, at T = 90 K). A different approach was taken for Xe and Pb recoil ions in LXe as described below. N_0 is given by $N_0 = \{(E/W_e)\cdot(1 + N_{ex}/N_i)\cdot(T_c/T)\}/R$, where W_e is the W-value for electrons, 23.6 and 15.6 eV in LAr and LXe, respectively. The N_{ex}/N_i ratios were taken to be 0.21 and 0.13 for LAr and LXe, respectively. a_0 values were calculated at E_{ini} for RHI, and $E_{ini}/2$ for other ions, where E_{ini} is the initial energy. The values of the interatomic distance a used in the calculation are 0.3865 and 0.48 nm for LAr and LXe, respectively. The energy E was replaced by E_η for slow recoils.

3.1. Fast Ions in Liquid Argon

Stopping power and ranges, 0.319 and 0.127 cm for ^{18}O and ^{36}Ar ions, respectively, were taken from SRIM [33]. Averaged LETs for ^{18}O and ^{36}Ar ions are 1.35 and 6.47 MeV·cm^2/mg, respectively. The energy expressed in MeV/n, and the velocity, for ^{18}O and ^{36}Ar ions, are practically the same as each other. The shape of the radial distribution is determined by the velocity. The difference is in the magnitude of the exciton density n_1. The initial core radii a_0 for ^{18}O and ^{36}Ar ions are almost the same, 1.53 and 1.49 nm, respectively. The T_c/T ratio is 0.75 for both ions. Averaged LET$_c$ for ^{18}O and ^{36}Ar ion cores are 1.01 and 4.85 MeV·cm^2/mg, respectively. The core density for ^{36}Ar ions is 5 times that for ^{18}O ions as shown in Figure 1b. Numerical calculations for the rate equations were performed to obtain q_c values.

The quenching factor q measured for 33.5 MeV/n ^{18}O is 0.59 and that for 31.9 MeV/n ^{36}Ar is 0.46, whereas calculated values for those ions are 0.71 and 0.44, respectively. The results obtained for 33.5 MeV/n ^{18}O and 31.9 MeV/n ^{36}Ar in liquid argon are shown as a function of the average LET together with results for other ions obtained previously in Figure 1a. These are 5.305 MeV α-particles, relativistic Ne, Fe, Kr, La and Au ions of 630 to 1.35 MeV/n. The T_s/T ratio of α-particles is 0.72, and that of relativistic heavy ions is 0.51 [15]. The results and constants used in the calculation are also shown in Table 1.

Table 1. Quenching factors calculated for ^{18}O, ^{36}Ar, Mo and Ba ions in liquid argon. Mo and Ba ions are for ^{252}Cf light fragments (LFs) and heavy fragments (HFs), respectively.

	Units	^{18}O	^{36}Ar	Mo (LF)	Ba (HF)
Energy	MeV/n	33.5	31.9	0.98	0.56
Range	μm	3200	1270	44	37
LET	MeVcm^2/mg	1.35	6.47	24.1	21.7
T_c/T		0.75	0.75	0.88	0.90
a_0	nm	1.53	1.49	1.52 [1]	1.46 [1]
q_c		0.64	0.27	0.083	0.087
q		0.73	0.46	0.19	0.18
q expt.		0.59 [2]	0.46 [2]	0.17 [3]	0.16 [3]

[1] Core expansion. [2] [16], [3] [12].

The q value obtained before using $\sigma_{HS}/4$ for LFs was 0.075 and is much smaller than the observed value of 0.17. LET for FFs is so high that a dense overlap of δ-rays occurs and contributes to the widening of the core. The T_s/T ratios were estimated to be 0.76 and 0.80, respectively. In addition to this, the density of excitons n_1 estimated by Equation (10) can exceed the atomic number density. Multiple ionization in the core very quickly degenerates into single ionizations by charge sharing with neighboring atoms [15]. Thus, the core quickly expands. The core radius is determined so that n_1 on the axis does not exceed the atomic number density. Therefore, an undifferentiating core, a single Gaussian distribution with $T_s/T = 1$, was assumed. However, the range for some δ-rays is still larger than the core radius. This may contribute to scintillation considerably. The averaged values 0.88 and 0.90 for LFs and HFs, respectively, were taken this time. Mo and Ba ions are considered for LFs (106.2 MeV) and HFs (80.3 MeV), respectively. The ranges, 31.4 and 26.5 μm, respectively, for LFs and HFs were obtained from SRIM. Averaged LETs are quite large, 2.41×10^4 and 2.17×10^4 MeVcm^2/g for LFs and HFs, respectively. The q_c values calculated are 0.083 and 0.087 and result in q_T values of 0.19 and 0.18 for LFs and HFs, respectively, agreeing well with experimental values.

The evolution of quenching in the track core produced in LAr by α-particles, ^{18}O and ^{36}Ar, Au and Ba (HF) ions is shown in Figure 3a. The initial core radii are a_0 = 0.39 and 5.8 nm for α-particles and Au ions, respectively, whereas those for ^{18}O and ^{36}Ar and Ba ions are ~1.5 nm. The evolution depends on both a_0 and LET in the track core.

It should be noted that the numerical results are well reproduced by Birks' law when the initial track core is constant, as demonstrated in the inverse plot in Figure 3b showing ${q_c}^{-1}$ values vs. LET in the core (LET_c). The q_c values calculated for ^{18}O and ^{36}Ar ions and the inverse values ${q_c}^{-1}$ are fitted as a function of LET_c. The data include trial calculations for evaluating uncertainty due to T_c/T ratio and are not shown in Figure 1a. The values are well fitted on a straight line that represents Birks' law. The values for Mo and Ba ions are also close to the extrapolated line. The results for RHIs also lie on a straight line. Using Equation (5) with normalized Birks' law, we obtain the following as a function of LET:

$$q = \frac{1}{1 + k_B B \cdot \{(T_c/T)LET\}} \cdot T_c/T + (1 - T_c/T) \tag{27}$$

The results are shown in Figure 1a. A dashed curve is a fitting by Birks' law for the RHIs, and the agreement of the two is quite good. The difference is not appreciable in Figure 1a, and therefore numerical results are not shown. Both give smaller values than measurements for Fe, Kr and La ions. The curves obtained for ^{18}O and ^{36}Ar ions are also shown. FFs were not included in the curve because of the difference in the T_c/T ratio.

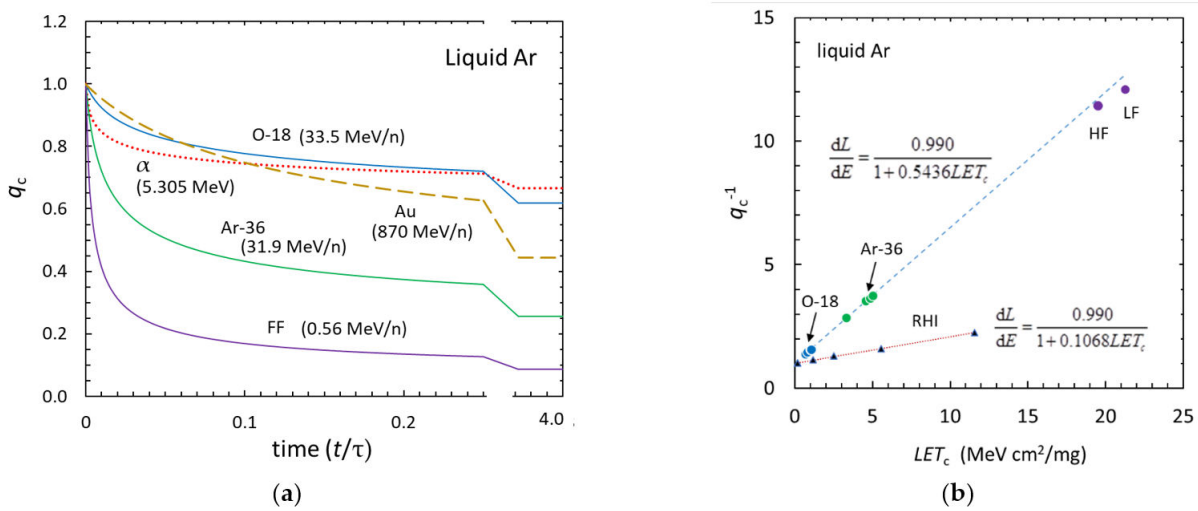

Figure 3. Calculated quenching in liquid argon. (**a**) Evolution of quenching in the track core produced by α-particles, Au, ^{18}O, ^{36}Ar and Ba ions (as heavy fission fragments). The ratio of the number of self-trapped excitons with and without quenching as a function of time is plotted. The initial radii are a_0 = 0.39 and 5.8 nm for α-particles (dotted curve) and Au ions (dashed curve), respectively. a_0 values for ^{18}O, ^{36}Ar and Ba ions (solid curves) are ~1.5 nm. (**b**) The inverse of q_c calculated for ^{18}O, ^{36}Ar, Mo (LF) and Ba (HF) ions plotted as a function of core LET. Birks' law was used to fit values for ^{18}O and ^{36}Ar ions. Birks' law applied for RHIs is also shown (a_0 = 5.4–6.2 nm).

3.2. Heavy Recoils in α-Decay in Liquid Argon

Studies for Ar recoils in LAr have been underway, and detailed descriptions and preliminary results are in arXiv [34]; therefore, Ar recoils in LAr are not treated here. The quenching model discussed in Section 2 can be applied for slow heavy ions in α-decay. The exciton density is given by replacing LET with LET_{el}. N_0 value is given by LET_{el}. The nuclear quenching factors q_{nc} calculated are compared with the experimental W_α/W_{NR} ratios in gas and shown in Figure 4a. The numerical calculation for Pb recoils in LAr by Lindhard et al. gives values significantly larger than the experimental values and those obtained by the power-law approximation. We took a semi-empirical power law by Ling and Knipp [30], Equation (25), which is similar to the power-law approximation by Lindhard; however, the coefficient was determined by using the measured W_α/W_{NR} ratios for a Ar + 5% air mixture by Madsen [27]. Measurements obtained for Ar by Jesse and Sadauskis [28] and measurements obtained for Ar + 2% CH_4 [29] and Ar + 2% Xe by Cano [29] are also shown. The agreements between the measurements are quite good.

Then, average LET_{el} was calculated simply by $LET_{el} = E_\eta/R = q_{nc}E/R$, where R is the range. Since the δ-ray energy is very small and its range is short, we assume all the energy is included in the core; T_c/T was taken to be 1, and $T_s = q_cT$. We obtained $N_0 = (E_\eta/W_e) \times (1 + N_{ex}/N_i)/R$. The exciton–ion ratio N_{ex}/N_i was taken to be 0.21. The calculations described in Section 2.2 were performed. The core radius r_B given by the Bohr criterion for slow recoil ions became smaller than the interatomic distance a, and then a value was taken for a_0. The density of exciton n_1 for Pb recoils exceeded the atomic number density. The core expansion had taken place, and a_0 was determined so that n_1 on the axis did not exceed the atomic number density.

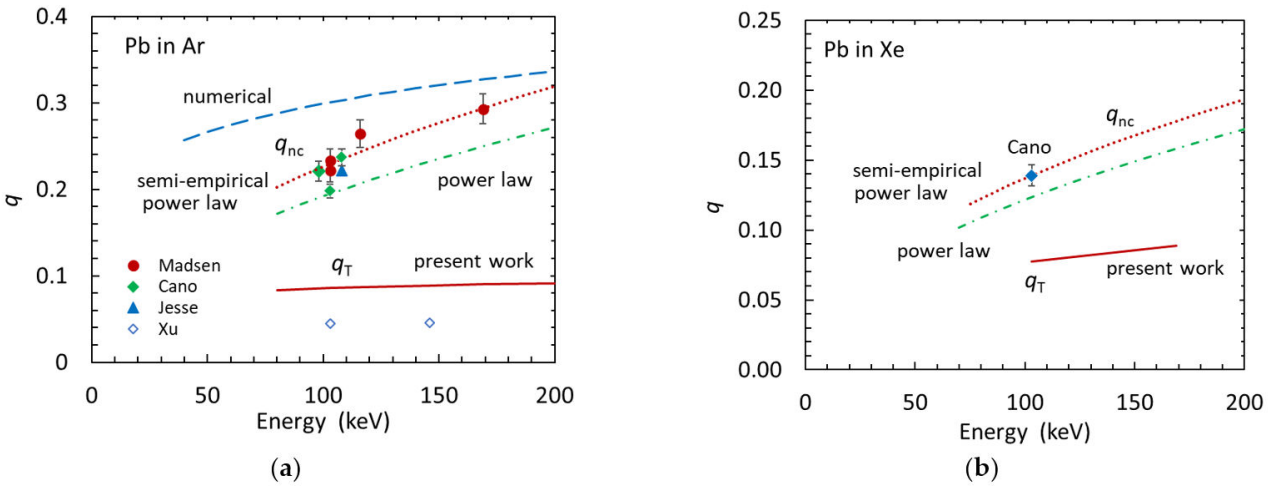

Figure 4. Quenching factors q_T and q_{nc} for heavy recoils in α-decay. (**a**) Quenching factors in liquid Ar. Calculations are for ^{208}Pb ions. Symbols are W_α/W_{NR} measurements in gas for ^{206}Pb, ^{208}Tl and ^{208}Pb ions by Madsen (•) [27]. Points for 103 keV ^{206}Pb recoil ions by Cano (closed diamond) [29] and Jesse and Sadauskis (triangle) [28] are shifted for clarity. Numerical results (dashed curve) and the power-law approximation (dot-dashed curve) for q_{nc} by Lindhard et al. are shown [23]. The dotted curve shows q_{nc} estimated by Ling and Knipp [30]. Measured q_T values by Xu et al. [35] are shown with open diamonds (corrected for $L_{\gamma 0}$) together with present calculation (solid curve). (**b**) Quenching factors in liquid Xe. W_α/W_{NR} measurements for ^{206}Pb in gas by Cano (closed diamond) [29]. Calculated values for q_{nc} are the power-law approximation (dot-dashed curve) by Lindhard et al. and the present approximation (dotted curve). The present calculation for q_T is shown by the solid line.

The calculated results for q_T show a slow increase, almost constant, represented by the energy increase shown in Table 2 and Figure 4a. q_{nc} increases with $E^{1/2}$, resulting in strong quenching at higher E, which compensates for the q_{nc} increase. As a result, the change in q_T with energy is small. The energy available for scintillation is $E_L = q_T \cdot E = q_{nc} \cdot q_{el} \cdot E$. The experimental values are the scintillation efficiency, L_{eff} (the nuclear recoil to gamma ratio, NR/γ), relative to 122 keV (or 59.5 keV) γ-rays. q_T is expressed as

$$q_T = L_{eff} L_{\gamma 0} \tag{28}$$

where $L_{\gamma 0}$ is the scintillation efficiency for γ-rays used as a reference. A value of $L_{\gamma 0} = 0.9$ in LAr is estimated using an S–Q plot, where S is the scintillation and Q is the charge collected, in [36]. The results are given in Table 1. Xu et al. reported that the 146 keV ^{210}Pb recoil ions an electron-equivalent energy of 7.4 ± 5 keV$_{ee}$ and the 103 keV ^{206}Pb recoil ions produce ~5 keV$_{ee}$ [35]. The scintillation efficiency of $L_{eff} = 1/19.7 = 0.051$, which is about one-half the value obtained here. They reported also that a ~5 keV$_{ee}$ signal is similar to a ~30 keV ^{40}Ar ion. They gave $L_{eff} = 1/6.2 = 0.16$ for ^{40}Ar ions. The present model gives $E_L = 6$ keV for 30 keV ^{40}Ar ions, and the signal ratio for the 103 keV ^{206}Pb recoil ions to 30 keV ^{40}Ar ions is about 1.5.

The energy spectrum taken for Pb recoils in LAr was previously reported [37]. The energy resolutions are Ω~12% and Ω~11% for ^{214}Pb recoils and ^{210}Pb recoils, respectively, while the power-law approximation gives the energy straggling in E_η of Ω~14%.

Table 2. Quenching factors q_T, q_{nc} and q_{el} and the energy available for scintillation, E_L, estimated for Pb and Tl ions in α-decay in liquid argon. The nuclear quenching factor q_{nc} was taken from Ling and Knipp [30]. E_L (keVee) = $E_L/L_{\gamma 0}$ (keV) = $E_L/0.9$ (keV).

Source		^{210}**Po**	^{212}**Bi**	^{214}**Po**	^{212}**Po**
Recoil Ion	**Units**	^{206}**Pb**	^{208}**Tl**	^{210}**Pb**	^{208}**Pb**
Energy	keV	103	116	146	169
R	μm	0.09	0.10	0.12	0.13
LET_{el}	MeVcm^2/mg	1.85	2.03	2.41	2.68
a_0	nm	0.45 [1]	0.47 [1]	0.51 [1]	0.54 [1]
q_{nc}		0.23	0.24	0.27	0.29
q_{el}		0.38	0.36	0.33	0.31
q_T		0.086	0.087	0.089	0.090
E_L	keV	8.9	10	13	15
E_L	keVee	10	11	14	17
E_L expt.	keVee	~5 [2]		7.4 ± 0.4 [2]	

[1] Core expansion. [2] Xu et al. [35].

3.3. Xe Recoils and Heavy Recoils in α-Decay in Liquid Xenon

An accurate set of constants, N_0, a_0, k (=σv), τ and D, needed for performing the numerical calculation discussed in Section 2 in LXe is not ready. Among them, the track constants, N_0 and a_0 may be estimated by R within certain uncertainties, if a reliable estimation of T_c/T ratio is made. The value of σ should be within a certain range, as discussed in the beginning of Section 3. However, a reasonable knowledge of exciton mass is needed to obtain k. The magnitude of τ can be 10^{-12} to 10^{-11} s, and the value of D has to be obtained from measurements. Since those constants have large uncertainties, if one can obtain them in a certain way, the results have to be compared with measurements. Experimental data available are quite few in LXe. Values of q for RHI fall off at about 6000 MeVcm^2/g in LAr, which gives a measure of the cross-section. However, existing data do not show the fall-off in LXe [38]. Large uncertainty enters in the T_c/T ratio for FFs to be used as a measure of the cross-section. Previously, we took the α-core approximation, in which a q_{el} value for Xe recoils is assumed to be the same as a q_c value for α-core [25]. In the present approximation, Birks' law was used to obtain quenching factors for Xe and Pb recoils in place of performing the numerical calculation discussed in Section 2.2. Birks' law reproduces the result of a second-order quenching reaction in heavy-ion track provided that the initial core radius is the same, as discussed in Appendix A and demonstrated in Figure 3b. It can be also applied for slow ions when dE/dr is replaced by LET_{el}. (=dE_η/dr). Birks' law includes two parameters, namely A and kB. However, there is only one experimental datum available to determine the parameters in liquid Xe, that for α-particles apart from those for RHIs, showing q = 1. Therefore, A is normalized as A = 1. The core radii given by the Bohr criterion are less than the interatomic distance for 5.49 MeV α-particles and Xe recoil energy less than 15 keV, so we set $a_0 = a$ for those ions. LET_{el} becomes large for Pb recoils, and then the core expansion is needed. Since the difference is small, 103 keV Pb recoils were treated as $a_0 \approx a$. The measured q for α-particles is 0.77 in LXe. Previously, we took the T_c/T ratio (0.72) for α-particles in LAr and obtained q_c = 0.68 for α-particles in LXe [25]. However, this underestimates the T_c/T value since r_B and a values are larger in LXe than in LAr. We took q = 0.77 and q_c = 0.70 with T_c/T = 0.76. Averaged LET for α-core is 0.327 MeVcm^2/mg. We took Equation (4), set A = 1 and then obtained a normalized form of Birks' law for electronic quenching:

$$q_{el} = \frac{dL}{dE_\eta} = \frac{1}{1 + 1.33 \cdot LET_{el}} \quad (29)$$

where LET_{el} is in MeVcm^2/mg. Equation (29) is only valid for ions with $r_B < a$ and when LET_{el} is not too large. It applies for Xe recoils in LXe at low energy. Birks' law, as a function

of LET_{el}, reproduces the result of the numerical calculations for slow ions in a LET_{el} region indicated with the solid curve in Figure 5a. The ratio a/a_0 for 169 keV Pb ions is 1.4 and is similar to the ratio in LAr; therefore, q_{el} value is corrected for the core expansion using results for 169 keV Pb ions by numerical calculation in LAr.

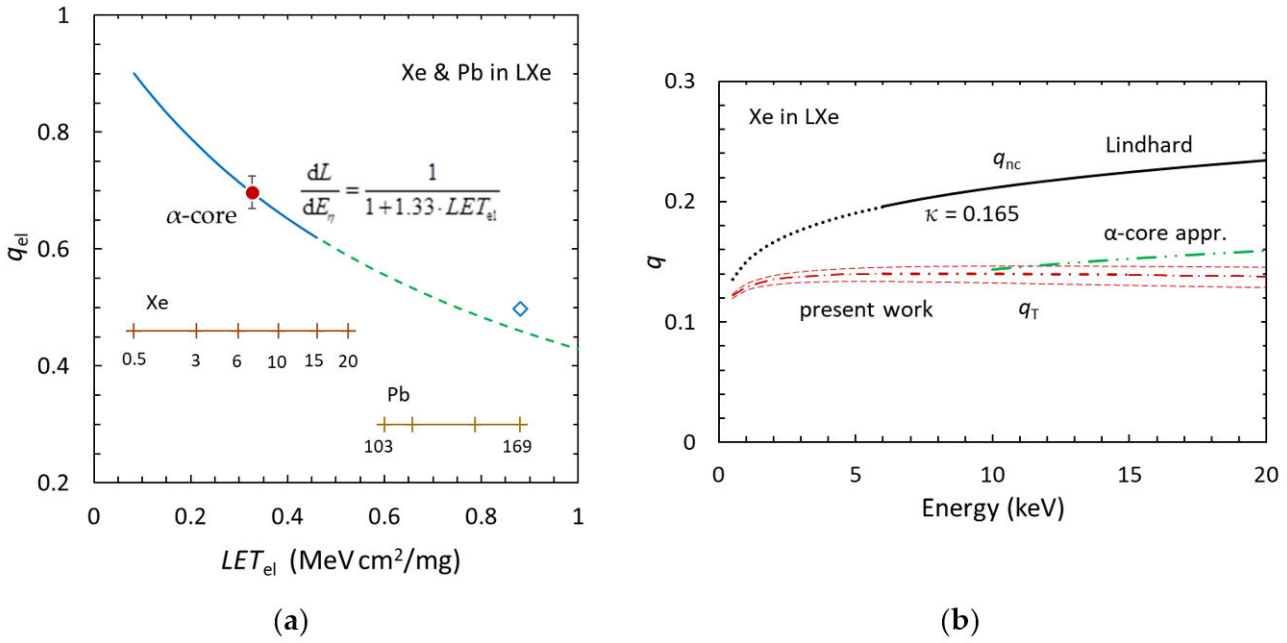

Figure 5. Quenching factors in liquid Xe: (**a**) The electronic quenching factor q_{el}, estimated for Xe and Pb recoils as a function of LET_{el}. A closed circle shows q_c = 0.70 for 5.49 MeV α-particle. Curves show Birks' law. Horizontal scales show the energy of Xe and Pb recoils in keV; the diamond show a value corrected for core expansion: (**b**) Quenching factors calculated for Xe recoils in liquid Xe as a function of the energy. The solid curve shows Lindhard q_{nc}, the dotted curve is an extrapolation. The dot-dashed curve shows the total quenching factor $q_T = q_{nc} \cdot q_{el}$. The dashed curves show uncertainties due to the estimated T_c/T ratio, 0.76 ± 0.04, in α track. The q_T curve may approach to Lindhard q_{nc} curve faster than the dot-dashed curve as the energy decreases below about 2 keV (see Sections 4.1 and 4.2). The result obtained previously by the α-core approximation is shown with a dot-dot dashed curve [25].

The total quenching factor q_T calculated for Xe recoils in LXe is almost constant, 0.14, down to about 3 keV and then shows a small decline, as shown in Table 3 and Figure 5b. The result obtained previously by the α-core approximation is also shown (dot-dot-dashed curve). The q_T with the α-core approximation decreases with q_{nc} as the energy decreases. The numbers of photons expected at zero field N_{ph0} is obtained as $(E_L/W) \times (1 + N_{ex}/N_i)$ $= E_L/(15.6\text{ eV}) \cdot 1.13$. Alternatively, $q_T \approx 0.14$ makes ~10 photons per keV for 3–15 keV. N_{ph0} basically gives the sum of the number of photons N_{ph} and number of electrons N_{el} under an external field (see the second paragraph in Section 4.3). The results for Pb recoils in LXe are shown in Figure 4b and listed in Table 3. q_T shows a gradual increase as the energy increases. A value of $L_{\gamma 0}$ = 0.89 in LXe was estimated using an *S*–*Q* plot, where *S* is photon and *Q* is charge collected [39], and was used to obtain E_L value in keVee. Measured q_T values for Xe in LXe quoted in [25] should be 0.89/0.77 = 1.15 times since a value for L_γ = 0.77 was used. Accordingly, the axis on the right in Figure 3 in [25] should be 1.15 times.

Table 3. Quenching factors q_T, q_{nc} and q_{el} and the energy available for scintillation, E_L, estimated for Xe recoils and Pb recoils in α-decay in liquid xenon. The q_{nc} values for Xe recoils are from Lindhard (k = 0.165) [23] and those for Pb recoils were obtained by the semi-empirical power-law approximation. Birks' law was exploited for obtaining q_{el} values. Related values for ^{241}Am α-core are also listed. E_L (keVee) = $E_L/L_{\gamma 0}$ (keV) = E_L/0.89 (keV).

Source				**^{210}Po**	**^{212}Po**	**^{241}Am**
Recoil Ion	**Units**	**Xe**	**Xe**	**^{206}Pb**	**^{208}Pb**	**α-Core**
Energy	keV	6	20	103	169	5490 × 0.76
R	μm	–	–	0.08	0.12	43
LET_{el}	MeVcm^2/mg	0.30	0.53	0.60	0.88	0.33
a_0	nm	0.48 [1]	0.51 [2]	0.55 [2]	0.66 [2]	0.48 [1]
q_{nc}		0.20	0.23	0.14	0.18	1
q_{el}		0.72	0.59	0.56	0.50 [3]	0.70
q_T		0.14	0.14	0.08	0.09	–
E_L	keV	0.8	2.8	8	15	–
E_L	keVee	0.9	3	9	17	–

[1] $a_0 = a$. [2] Core expansion. [3] Corrected for core expansion.

4. Discussion

4.1. Fast Ions in Liquid Argon

The results computed with the hard-sphere cross-section divided by 4, $\sigma_{HS}/4$ = 43 Å^2, for fast ions in LAr provide a reasonable agreement with the experimental data as seen in Figure 1a. The most noticeable departure of the calculation from the experiment is in the case of relativistic heavy ions. The measured scintillation efficiency q for Ne to La is almost 1, and that for Au is 0.70–0.76 [12]. A flat response is seen in LET up to about 6000 MeVcm^2/g then falls off. The present model shows that q decreases gradually as LET increases. Birks' law also predicts a gradual decrease towards high LET. It has been pointed out that NaI(Tl) and CsI(Tl) show a flat-top and then fall off [40,41] as LET increases. The scintillation efficiency shows a flat response in LET up to ~100–200 MeVcm^2/g in these inorganic crystals. This type of behavior cannot be interpreted within the framework of the present model or a model by Murray and Mayer for activated ionic crystals [40]. Inclusion of a higher-order term, $(dE/dr)^2$, in the denominator in Equations (3) and (4) may reproduce the experimental curve for RHI; however, that would not explain the response to other ions. The inclusion of a second-order term will result in a strong quenching for α-particles, ^{18}O and ^{36}Ar ions, which have much higher exciton density than that seen in RHI tracks (Figure 1b). An expanded Birks' law may include a second-order term; however, that is to interpret behaviors in the small q region in high LET. The biexcitonic reaction model requires recombination to occur prior to thermalization. Evidence shows that this indeed happens: the thermalization time for LAr is ~1 ns for electron excitation, but recombination occurs much faster in α-excitation [17]. It has been discussed how the cylindrical field due to a high linear density of positive charge on the track axis plays a key role to prompt recombination [15]. The quenching mechanism assumes the cylindrical structure. The tracks for RHIs are so broad that an electron produced in the track core would not feel the cylindrical field caused by charges on the track axis.

The result for ^{36}Ar ions agrees quite well with the measurement. However, calculation gives considerably larger q for ^{18}O. The ranges for ^{18}O and ^{36}Ar ions are long, 3.2 and 1.27 mm, respectively. The ion beams were introduced towards the PMT. A simple but strong correction for the solid angle against PMT had been made. The q values without the correction are 0.67 and 0.48, respectively. When q becomes small, uncertainty in the T_c/T ratio affects the final results. The uncertainties for FFs are mostly due to that in the T_c/T ratio.

Evolution of quenching, the ratio of the number of self-trapped excitons with and without quenching, as a function of time is plotted for the track core produced by α-

particles, Au, ^{18}O, ^{36}Ar and Ba ions (as HFs) in Figure 3a. Quenching tends to proceed strongly at first and then becomes slow. The effect due to the difference in the track core radius is seen for α-particles (a_0 = 0.39 nm) and Au ions (a_0 = 5.8 nm). Quenching proceeds significantly in a very short time and then proceeds quite slowly for α-particles, while quenching proceeds slowly but persists for a long time for Au ions. The radii for ^{18}O, ^{36}Ar and Ba ions can be regarded as the same (a_0 = 1.5 nm), as shown in Figure 1b; however, the evolution of quenching is different. Quenching is very severe in the beginning in the core with high excitation density. The evolution of quenching depends on both a_0 and n_1.

The photoionization mechanism had been investigated for a high-energy-resolution detector for heavy ions of 20–100 MeV/n [13,14,42], which can be quite useful in nuclear physics and evaluation of radiation in manned spacecraft. Measurements in a small detector showed expecting results [13], and then measurements in a larger prototype detector were performed [42]. However, the expected results were not obtained. The concentration of doping agent should be on the order of a few ppm when the detector is large enough [43,44]. Otherwise, the collisional energy transfer exceeds the photoionization; when this happens, the space charge effect is strong and may degrade the energy resolution in a very high LET region [42]. More investigation is needed to a draw conclusion on the performance of PID.

4.2. Recoil Ions in Dark Matter Searches

Measurements for Pb recoils in noble liquids are few. The q_T values reported for 103 and 146 keV Pb ions in LAr by [35] are almost one-half those obtained in the present calculations. The scintillation measurements are often influenced by the position of ionization in a detector due to the reflection, the quantum efficiencies of the wavelength shifter and PMT, the solid angle to PMT, etc. However, a discrepancy by a factor of 2 seems to be too large. The range R is mostly determined by S_{nc}; the stopping power theories for the elastic scattering is not as bad for ~100 keV Pb recoils. Errors in R may be compensated by the consequential change in q_{el}; therefore, an influence on the q_T value may not be significant. The measured W_α/W_{NR} values agree with each other [27–29]. More measurements are necessary both in LAr and LXe. The difference in q_{nc} between the numerical calculation and the power-law approximation by Lindhard for Pb recoils in Ar is quite large, as shown in Figure 4a. The numerical calculation ought to give better values than the power-law approximation since the potential used is more realistic. However, the experimental values lie in between and even nearer to the power-law approximation at about 100 keV. The continuous slowing down approximation (CSDA) was used in the numerical calculation as in most numerical calculations; however, the number of collisions, excitation and ionization produced may not be enough for such a complex system. Monte Carlo simulations such as the TRIM package in principle suit cases with $Z_1 \neq Z_2$, where theoretical evaluation is quite difficult. Pb recoils in LAr can be an excellent test for simulations.

The present results for q_T for Xe recoils in LXe show an almost flat response to the energy. Results obtained for RHI suggest that q_{el} increases more rapidly than a second-order reaction kinetics predict when q_{el} nears 1. Therefore, at very low energy, it is possible that q_T approaches the Lindhard q_{nc} more rapidly than is shown in Figure 5b. The experimental results reported for slow Xe recoils in LXe are scattered and complicated. Model-dependent analyses were often conducted to obtain the q values. In contrast, the present results are simple, as listed in Table 3 and shown in Figure 5b. One can compare the present results with any experimental results easily. Therefore, the results are not compared with the measurements. Some of the theoretical evaluation of q_T, including the TRIM package, in low energy recoil Xe in LXe is compared [45] together with the experimental relative scintillation efficiency. The present results seem to give larger q_T values at energy lower than about 6 keV, although there can be errors in experiments. Many reasons can be thought of to increase theoretical q_T values for Xe-Xe since LET_{el} becomes small and the range becomes very short and the track is not straight but has branches. Measurements for Pb recoils will provide useful information on the effect of the range. There are few effects that may reduce the q_T values in low energy. One is uncertainty in q_{nc}. Barker and Mei [46]

compared theoretical models for ionization efficiency for germanium with experimental data down to 1 keV or less. Although experimental data scatter, they concluded that there is a fair agreement between the Lindhard model ($\kappa = 0.159$) and experimental data at low energy. An ε value for 1 keV Ge-Ge is 0.0035, which corresponds to 3.4 keV for Xe-Xe. Uncertainty due to T_c/T for α-particles in LXe is $0.72 \leq T_c/T \leq 0.80$ with systematic uncertainty of $\pm 6\%$.

The systematic uncertainty in theory is difficult to assess. Setting a_0 equal to a when r_B is smaller than a is artificial, and the effects of this simplification are not clear. The largest uncertainty is due to the nuclear quenching factor q_{nc}, which directly influences the q_T value. Uncertainty in q_{nc} for Xe-Xe in $6 \leq E \leq 20$ keV can be roughly $+15/-40\%$. Meanwhile, q_{el} depends on q_{nc} and R. The Thomas–Fermi treatment for the stopping power theories becomes a crude approximation at very low energy ($\varepsilon < 0.01$) (see [47], p. 10), which corresponds to 10 keV in Xe-Xe collisions, when the ion and the atom do not come close to each other. Moreover, the electronic excitation and scattering are correlated in slow ion–atom collisions. The orbital electron can adjust itself for the projectile and target motion in the collision process and forms a transient molecular orbit [48,49]. It is not treated in Lindhard's theory. Other theories proposed are no better than the Lindhard theory [23] in this sense. The W-value measurements in gas phase should be performed to obtain experimental q_{nc}. Guillaudin et al. measured W values for slow ions in low-pressure gases; however, they are still limited for small Z ions [50]. Measurements of the W_α/W_{NR} ratio, which gives q_{nc}, in high-pressure gas (≤ 0.2 g/cm^3) [51,52] by neutron scattering could give direct and most reliable information. The experimental scintillation efficiency is relative to 122 keV (or 59.5 keV) γ-rays. Accurate values for scintillation efficiency for these γ-rays are required.

4.3. General Remarks on Dark Matter Searches

A large-scale two-phase noble gas TPC as a dark matter detector operates with the external field and uses the sum of the scintillation S and the charge Q signals. The analysis of data in dark matter detectors relies on a complementary relationship between S and Q; a proper summation of the two gives the constant quenching factor q_T as a function of the electric field. A parameterized Jaffé theory $Q(F) = Q_0/(1 + k_J/F)$, where $Q(F)$ is the charge collected at the electric field F and $Q_0 = N_i$ in the unit of electrons is often used [53]. The coefficient k_J represents the strength of recombination, and it depends on the energy and the kind of charged particles. The relationship is often in use to calibrate TPCs for dark matter searches (see [2], pp. 26−31). Although the relationship may be used for high F, fitting it to data in low F and extrapolating the results to high F to obtain Q_0, in other words, to use it for calibration, is quite questionable. As a result, a value of $N_{ex}/N_i = 1$, which is not impossible but not very likely, for slow recoils is reported. A value of $N_{ex}/N_i = 1$ also demands a change in W_{NR}. The N_{ex}/N_i ratio for electrons in LAr (0.21) is reliable since a value given by Penning ionization measurements and a value obtained by the optical approximation agreed. For LXe, the theory (0.06) and the measurement by Q vs. S plot (0.20) disagree; therefore, an average value, 0.13, was taken here. The same ratios were used for α-particles and slow recoils. The difference in the N_{ex}/N_i ratio in this range would not affect the final results significantly, since the q_T values obtained are almost constant with energy. W values for heavy noble gases, Ar, Kr and Xe, hardly depend on the energy and the type of the particles. Heavy noble liquids do not have metastable states, and the energy of the excited states is close to the ionization energy. Therefore, strong evidence is needed to accept the value of $N_{ex}/N_i = 1$.

An abrupt collection of charge and a very weak dependence of the charge yield on the electric field is reported for ~50−100 keV recoils and was attributed to the escape electrons in some cases. However, LET_{el} values for these recoils are quite high. The q_T values for ^{18}O and ^{36}A ions in LAr have been observed to increase by ~22–24% at about 3 kV/cm, as shown in Figure 1a [14]. The field effects observed for ^{18}O and ^{36}A ions could occur for slow recoils for dark matter searches in LAr and LXe. The behavior was attributed to the

recovery of quenching with the field. The increase saturates at a relatively low field, and the total recovery has not been reported [54]. However, the effects have not been noticed in the data analysis in noble liquid TPCs. The field effect will be discussed elsewhere.

Simulations are powerful and indispensable tools to analyze data obtained in a large scale detector. However, it is important to have reliable information for fundamental processes and accurate constants, such as collision cross-sections and saturation characteristics of charge yield in low energy. Many of these are missing. Theories become quite hard and almost impossible without information from measurements for slow ions. Some values have to be obtained by experiment. More data and more work to understand the fundamental behavior are urgently needed. In particular, measurements of the W_α/W_{NR} ratio in high-pressure gas is crucial. Birks' law applied for Xe recoils in LXe, Equation (29), is independent of q_{nc} (or E_η). When a reliable stopping power S_T and q_{nc} are available, Equation (29) and the curve in Figure 5a are used to obtain q_{el} by modifying the energy scale in Figure 5a by Equation (19). Then, the total quenching factor is given by $q_T = q_{nc} \cdot q_{el}$. It is a straightforward procedure. A measured W_α/W_{NR} ratio will drastically reduce the systematic uncertainty in q_T for Xe recoils in LXe.

4.4. Birks' Law and Second-Order Reaction Kinetics

Birks' law has been reinvestigated in relation to reaction kinetics with consideration of the track structure, and the dependence on the track radius was studied for the first time. Birks' law represents various reactions: first-order reactions as well as second-order reactions with diffusion. An approximate equation, Equation (16), was derived for the biexcitonic collision kinetics discussed in Section 2.2 (Appendix A). Birks constants, k_B, A and B, are related to the reaction rate k, the diffusion constant D, the density of excitons n_1, the specific number N_0 and the initial radius a_0. The new evidence makes the scaling law possible as well as an extrapolation of experimental data. The approximate equation was compared with the numerical calculation for heavy ions in LAr. The agreements were moderate, 3% to 20%, depending on the track radius and the exciton density since the approximations are crude. However, it is found that Birks' law reproduces the numerical results quite well, within 2% or less, when it is used properly as a fitting function. Birks' law is applied for quenching in the track core to obtain q_c in Equation (5), as in Figure 3b, and then Equation (27) is used to obtain q as a function of LET for heavy ions, as in Figure 1a.

A second-order kinetics has been discussed before for scintillation quenching in anthracene [19], NaI(Tl) and CsI [40,55,56]. Blanc and Birks [19] used a differential equation close to the present model, Equation (A5), with anthracene [55]. Salamon and Ahlen proposed a second-order annihilation of "excitons" (or electron–hole pairs) in NaI(Tl). Their model includes the initial dose profile and diffusion of excitons. The track structure they used was different from a core–penumbra structure in the present model. The characteristics and behavior of an exciton are different from these discussed here for noble liquids. The exciton motion is treated as coherent, where $D = 1$ cm^2/s and $k = 5 \times 10^{-8}$ cm^3/s in LAr, whereas the exciton motion is treated as diffusive in anthracene and NaI(Tl); e.g., $D = 1 \times 10^{-4}$ cm^2/s and $k = 4 \times 10^{-12}$ cm^3/s in NaI(Tl). The exciton lifetime τ is ~1 ps in LAr and ~15 ns in NaI(Tl).

Birks' law gives satisfactory agreements for many organic and inorganic scintillators without attention to the velocity (or the energy in MeV/n). The electronic states, scintillation and quenching mechanisms are complex in these scintillators. Moreover, these scintillators are not as strong as noble liquids against quenching. This may make the dependence of the track radius on Birks' law low.

Applications of Birks' law for low-energy recoils in noble liquids have been reported. However, S_T or S_e was used, and discussion of the quenching mechanism was not given. Birks' law was used as a fitting function. The Birks constants, A and B, relate N_0 and n to dE/dx. Therefore, LET_{el} ($= -dE_\eta/dx$) should be used for slow recoils, since E_η is the energy available for ionization and excitation. Birks' law was used here to obtain the scintillation

yield in LXe, and this usage is not a fitting. No experimental data in a keV region have been used. The use of Birks' law presented here is equivalent to performing numerical calculations for a second-order reaction with diffusion although individual constants are not given. The following comments may be noted for using Birks' law in place of numerical calculations:

1. The radius of the initial ion track core should be regarded as constant since the reaction kinetics include the density n, not the specific number N.
2. The boundary for kinetics, the track structure of heavy ions, has to be considered.
3. LET_{el}, not S_{e} or S_T, should be used in place of $\mathrm{d}E/\mathrm{d}r$ in Birks' law for slow recoils.

5. Conclusions

Biexcitonic collision kinetics with prescribed diffusion using a core–penumbra track model has been applied for various ions in a wide range of energy in liquid argon. In spite of their short lifetime (~1 ps), the free excitons are responsible for scintillation quenching in noble liquids. Agreements with measurements were obtained with a quarter hard-sphere cross-section. It is found that Birks' law reproduces the biexcitonic collision kinetics with diffusion quite well when the initial track radius is regarded as constant. This feature was used to evaluate the scintillation efficiency for 0.5–20 keV recoil Xe in liquid xenon, which is crucial in WIMP searches as well as the search for CEνNS events in next-generation multi-ton LXe TPCs. This model uses the scintillation efficiency in α-track core, unlike the usual use of Birks' law, and contains no free adjustable parameters. The density of excitons produced by Xe recoils needed for the calculation was given by electronic LET. Measurements of the W_α/W_{NR} ratio in gas phase to obtain a reliable nuclear quenching factor are urgently needed.

Funding: This research received no external funding.

Acknowledgments: The author would like to thank M. Yamashita for providing information on dark matter experiments and K.D. Nakamura for valuable discussions. The author is grateful to J.A. Laverne and E. Shibamura for reading the manuscript and for useful suggestions. The author thanks J. Xu for providing information on their experiments.

Conflicts of Interest: The author declares no conflict of interest.

Abbreviations

CEνNS	coherent elastic neutrino-nucleus scattering
CSDA	continuous slowing down approximation
FFs	fission fragments
FWHM	full width at half maximum
HFs	heavy fragments
keVee	electron recoil equivalent energy in keV
LAr	liquid argon
LET	linear energy transfer ($-\mathrm{d}E/\mathrm{d}x$)
$\mathrm{LET_c}$	linear energy transfer in the track core
$\mathrm{LET_{el}}$	electronic linear energy transfer
LFs	light fragments
LXe	liquid xenon
NR	nuclear recoil
PET	positron emission tomography
PID	photoionization detector
PMT	photomultiplier tube
RC Ar	recoil argon
RHI	relativistic heavy ion
TPC	time projection chamber
VUV	vacuum ultraviolet
WIMPs	weakly interacting massive particles

Appendix A

Birks' Law and Reaction Kinetics

Birks' law may be applied for many scintillators, and different kinds of quenching mechanisms have been proposed. We discuss two typical cases, as illustrated in Figure 1. The first case is the authors' interpretation of the original Birks' law [18]. The second case is the present model and is similar to the Blanc–Birks model (see [19], pp. 197–200), where level 1 fluoresces.

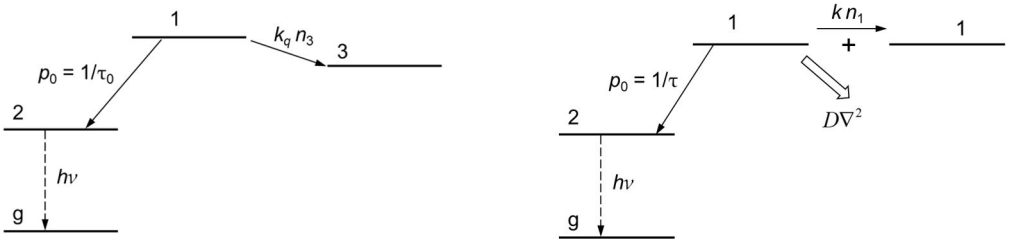

Figure 1. Schematic drawing of quenching. Level 1 is the excited level involved in quenching, level 2 gives fluorescence and level 3 is the quencher. (**a**) Pseudo-first-order reaction. (**b**) Second-order reaction under diffusion.

1. Pseudo-first-order reaction

Birks' law was originally proposed as capture of an excitation (level 1 in Figure 1a) by a damaged molecule (level 3) [18]. Level 2 is an excited level in the molecule, or undamaged molecule, that gives fluorescence. The differential equation after the charged particle incident would be as follows:

$$\mathrm{d}n_1/\mathrm{d}t = -p_0 n_1 - k_q n_1 n_3 \tag{A1}$$

where n_1 and n_3 are the density of excitation and damaged molecules, respectively, in a cylindrical track; p_0 is the decay rate without quenching; and k_q is the rate of capture. The equation may be treated as a pseudo-first-order reaction as a usual procedure ($n_1 << n_3$ and/or $\tau_1 << \tau_3$). The decay is exponential with the decay rate p given as

$$p = p_0 + k_q n_3 \tag{A2}$$

The scintillation efficiency, the ratio of intensity I_q to I_0 with and without quenching, is expressed as the ratio of rate constants with and without quenching as

$$\frac{I_q}{I_0} = \frac{n_{10}\int \mathrm{e}^{-pt}\mathrm{d}t}{n_{10}\int \mathrm{e}^{-p_0 t}\mathrm{d}t} = \frac{p_0}{p} = \frac{1}{1+(k_q/p_0)n_3} \tag{A3}$$

where n_{10} is the initial density of level 1. When the radius of the track is assumed constant, the number of excitons produced per unit length is proportional to specific energy loss, $A\mathrm{d}E/\mathrm{d}r$. The local concentration of damaged molecules is also proportional to specific energy loss, $B\mathrm{d}E/\mathrm{d}r$. Then, the specific fluorescence is given by Birks' law:

$$\frac{\mathrm{d}L}{\mathrm{d}r} = \frac{A\mathrm{d}E/\mathrm{d}r}{1+k_\mathrm{B}B\mathrm{d}E/\mathrm{d}r} \tag{A4}$$

where $k_\mathrm{B} = k_q/p_0$ is proportional to the exciton capture probability of a damaged molecule, relative to an undamaged molecule. The effect of a first-order reaction is to shorten the lifetime of the level involved in quenching. When level 1 is the level that fluoresces, p_0 includes the radiative decay rate. The scintillation decay shows a shortened lifetime, $1/\tau = 1/\tau_0 + k_q n_3$. On the other hand, if level 2 is the level that fluoresces, as illustrated in Figure 1a, the shortened time appears in the rise time of the scintillation (when $\tau_1 < \tau_2$).

2. Second-order reaction under diffusion

The differential equation to a second-order reaction illustrated in Figure 1b is given as Equation (8):

$$\partial n_1/\partial t = D\nabla^2 n_1 - n_1/\tau - kn_1^2 \tag{A5}$$

The solution is given as discussed in Section 2.2 using a normalized Gaussian radial distribution:

$$N(t) = N_0 e^{-t/\tau}\left[1 + \frac{kN_0}{2\pi}\int_0^t \frac{\exp(-t'/\tau)dt'}{a_0^2 + 4Dt'}\right]^{-1} \tag{A6}$$

where N_0 is the initial number of excitons per unit length. The integration is written as Equation (12):

$$N(t) = N_0 e^{-t/\tau}\left[1 + \frac{kN_0}{2\pi}\cdot\frac{\exp(u_0)}{4D}\{E_1(u_0) - E_1(u_t)\}\right]^{-1} \tag{A7}$$

where $E_1(\xi)$ is the exponential integral

$$E_1(\xi) = \int_\xi^\infty \frac{e^{-\xi}}{\xi}d\xi, \text{ and } u_0 = \frac{a_0^2}{4D\tau},\ u_t = \frac{a_0^2 + 4Dt}{4D\tau}. \tag{A8}$$

Equation (A7) represents the decay of free excitons. We compare N(t) and N_{nq}(t), with and without biexcitonic collisions, to obtain the quenching factor q as

$$q \simeq \frac{N(t)}{N_{nq}(t)} = \frac{N_0 e^{-t/\tau}}{N_0 e^{-t/\tau}}\left[1 + \frac{kN_0}{2\pi}\cdot\frac{\exp(u_0)}{4D}\{E_1(u_0) - E_1(u_t)\}\right]^{-1} \tag{A9}$$

For $t >> \tau$. $E_1(u_0) >> E_1(u)$, we approximate as

$$q \simeq \frac{1}{1 + k\cdot\frac{\exp(u_0)}{8\pi D}E_1(u_0)\cdot N_0} \tag{A10}$$

Consider another way of approximation. The emission is from the self-trapped exciton (level 2). The population of self-trapped exciton per unit length N_2 is given by Equation (14) as

$$N_2(t) = \int_0^t \frac{N(t')}{\tau}dt' = N_0\int_0^t \frac{e^{-t'/\tau}}{\tau}\left[1 + \frac{kN_0}{2\pi}\cdot\frac{\exp(a_0^2/4D\tau)}{4D}\{E_1(u_0) - E_1(u_t)\}\right]^{-1} dt' \tag{A11}$$

Since $E_1(u_0) >> E_1(u)$ except at a very small t, then $E_1(u) \to 0$. We approximate (see [19], pp. 185–234) as follows:

$$N_2(\infty) \simeq N_0\left[1 + \frac{kN_0}{2\pi}\cdot\frac{\exp(a_0^2/4D\tau)}{4D}E_1(u_0)\right]^{-1}\int_0^\infty \frac{e^{-t'/\tau}}{\tau}dt' \tag{A12}$$

Then, the approximate value for q is given by dividing Equation (A12) by N_0:

$$q \simeq \frac{1}{1 + k\cdot\frac{\exp(u_0)}{8\pi D}E_1(u_0)\cdot N_0} \tag{A13}$$

Equation (A13) is the same as Equation (A10). As N_0 is proportional to dE/dr, we write $N_0 = B(dE/dr)$. We have the following normalized form of Birks' law:

$$\frac{dL}{dE} = \frac{1}{1 + k\cdot\left[\frac{\exp(u_0)}{8\pi D}E_1(u_0)\right]\cdot B\frac{dE}{dr}} \tag{A14}$$

when the initial radius a_0 of the track can be regarded as constant. We rewrite $k_B = k \cdot [\ ]$. The decay of scintillation emission of a second-order reaction will be nonexponential. When level 1 is the level that fluoresces, p_0 includes the radiative decay rate. Blanc and Birks predicted a spike in the scintillation decay [19]; however, the spike was not reported. If level 2 is the level that fluoresces, as illustrated in Figure 1b, the sharp rise will appear and then an exponential decay of level 2 will follow.

For slow recoils, dE/dr is replaced by dE_η/dr, the electronic LET, as $N_0 = (LET_{el}/W_e) \times (1 + N_{ex}/N_i)/R$, where W_e is the W-value for electrons and N_{ex}/N_i is the ratio of produced excitons to ionization. Birks' law may be applied to many types of reactions; in other words, Birks' law does not tell the type of reaction that is involved. Observation of the scintillation decay, as well as quantitative studies, is needed to determine the quenching mechanism.

References

1. Aprile, E.; Doke, T. Liquid xenon detectors for particle physics and astrophysics. *Rev. Mod. Phys.* **2010**, *82*, 2053–2097. [CrossRef]
2. Chepel, V.; Araujo, H. Liquid noble gas detectors for low energy particles. *JINST* **2013**, *8*, R04001, and references therein. [CrossRef]
3. Suzuki, S.; Hitachi, A. Application of rare gas liquids to radiation detectors. In *Charged Particle and Photon Interactions with Matter: Recent Advances, Applications, and Interfaces*; Hatano, Y., Katsumura, Y., Mozumder, A., Eds.; Taylor & Francis: Boca Raton, FL, USA, 2010; Chapter 31; pp. 879–922.
4. Aprile, E.; Aalbers, J.; Agostini, F.; Alfonsi, M.; Amaro, F.D.; Anthony, M.; Antunes, B.; Arneodo, F.; Balata, M.; Barrow, P.; et al. (XENON collaboration). The XENON1T dark matter experiment. *Eur. Phys. C* **2017**, *77*, 881. [CrossRef]
5. Barrow, P.; Baudis, L.; Cichon, D.; Danisch, M.; Franco, D.; Kaether, F.; Kish, A.; Lindner, M.; Undagoitia, T.M.; Mayani, D.; et al. Qualification test of the R11410-21 photomultiplier tubes for the XENON1T detector. *J. Instrum.* **2017**, *12*, P01024. [CrossRef]
6. Akerib, D.S.; Alsum, S.; Araújo, H.M.; Bai, X.; Bailey, A.J.; Balajthy, J.; Beltrame, P.; Bernard, E.P.; Bernstein, A.; Biesiadzinski, T.P.; et al. (LUX collaboration). Low-energy (0.7–74 keV) nuclear recoil calibration of the LUX dark matter experiment using D-D neutron scattering kinematics. *Phys. Rev. Lett.* **2017**, *118*, 021303. [CrossRef]
7. Tan, A.; Xiao, M.; Cui, X.; Chen, X.; Chen, Y.; Fang, D.; Fu, C.; Giboni, K.; Giuliani, F.; Gong, H.; et al. (PandaX-II collaboration). Dark matter results from first 98.7 days of data from the PandaX-II experiment. *Phys. Rev. Lett.* **2016**, *117*, 121303. [CrossRef]
8. Agnes, P.; Albuquerque, I.F.; Alexander, T.; Alton, A.K.; Araujo, G.R.; Ave, M.; Back, H.O.; Baldin, B.; Batignani, G.; Biery, K.; et al. (DarkSide Collaboration). DarkSide-50 532-day dark matter search with low-radioactivity argon. *Phys. Rev. D* **2018**, *98*, 102006. [CrossRef]
9. Lenardo, B.G.; Xu, J.; Pereverzev, S.; Akindele, O.A.; Naim, D.; Kingston, J.; Bernstein, A.; Kazkaz, K.; Tripathi, M.; Awe, C.; et al. Low-energy physics research of xenon detectors for nuclear-recoil-based dark matter and neutrino experiments. *Phys. Rev. Lett.* **2019**, *123*, 231106. [CrossRef]
10. Akimov, D.; Albert, J.B.; An, P.; Awe, C.; Barbeau, P.S.; Becker, B.; Belov, V.; Brown, A.; Bolozdynya, A.; Cabrera-Palmer, B.; et al. (COHERNT collaboration). Observation of coherent elastic neutrino-nucleus scattering. *Science* **2017**, *357*, 1123–1126.
11. Tayloe, R. (COHERENT collaboration). The CENNS-10 liquid argon detector to measure CEvNS at the spallation neutron source. *arXiv* **2018**, arXiv:1801.00086.
12. Doke, T.; Crawford, H.J.; Hitachi, A.; Kikuchi, J.; Lindstrom, P.J.; Masuda, K.; Shibamura, E.; Takahashi, T. LET dependence of scintillation yields in liquid argon. *Nucl. Instrum. Methods Phys. Res. Sect. A* **1988**, *269*, 291–296. [CrossRef]
13. Hitachi, A.; LaVerne, J.A.; Kolata, J.; Doke, T. Energy resolution of allene doped liquid argon detectors for ions of energy 23–34 MeV/amu. *Nucl. Instrum. Methods Phys. Res. Sect. A* **1994**, *340*, 546–550. [CrossRef]
14. LaVerne, J.A.; Hitachi, A.; Kolata, J.J.; Doke, T. Scintillation and ionization in allene-doped liquid argon irradiated with ^{18}O and ^{36}Ar ions of 30 MeV/u. *Phys. Rev. B* **1996**, *54*, 15724–15729. [CrossRef]
15. Hitachi, A.; Doke, T.; Mozumder, A. Luminescence quenching in liquid argon under charged-particle impact: Relative scintillation yield at different linear energy transfers. *Phys. Rev. B* **1992**, *46*, 11463–11470. [CrossRef]
16. Hitachi, A. Exciton kinetics in condensed rare gases. *J. Chem. Phys.* **1984**, *80*, 745. [CrossRef]
17. Hitachi, A.; Takahashi, T.; Funayama, N.; Masuda, K.; Kikuchi, J.; Doke, T. Effect of ionization density on the time dependence of luminescence from liquid argon and xenon. *Phys. Rev. B* **1983**, *27*, 5279–5285. [CrossRef]
18. Birks, J.B. Scintillations from organic crystals: Specific fluorescence and relative response to different radiations. *Proc. Phys. Soc.* **1951**, *64*, 874–877. [CrossRef]
19. Birks, J.B. *The Theory and Practice of Scintillation Counting*; Pergamon: Oxford, UK, 1964.
20. Chatterjee, A.; Shaefer, H.J. Microdosimetric structure of heavy ion tracks in tissue. *Radiat. Environm. Biophys.* **1976**, *13*, 215–227. [CrossRef]
21. Mozumder, A. *Fundamentals of Radiation Chemistry*; Academic: San Diego, CA, USA, 1999.
22. Lindhard, J.; Winther, A. Stopping power of electron gas and equipartition rule. *Fys. Medd. Dan. Vid. Selsk.* **1964**, *34*, 1–21.

23. Lindhard, J.; Nielsen, V.; Sharff, M.; Thomsen, P.V. Integral equations governing radiation effects. *Mat. Fys. Medd. Dan. Vid. Selsk.* **1963**, *33*, 1–42.
24. Biersack, J.P. Range of recoil atoms in isotropic stopping materials. *Eur. Phys. J. A* **1968**, *211*, 495–501. [CrossRef]
25. Hitachi, A. Properties of liquid xenon scintillation for dark matter searches. *Astropart. Phys.* **2005**, *24*, 247–256. [CrossRef]
26. Hitachi, A. Bragg-like curve for dark matter searches: Binary gases. *Radiat. Phys. Chem.* **2008**, *77*, 1311–1317. [CrossRef]
27. Madsen, B.S. Ionization measurements on single recoil particles from Po, ThC, and ThC′. *Mat. Fys. Medd. Dan. Vid. Selsk.* **1945**, *23*, 1–16.
28. Jesse, W.P.; Sadauskis, J. Recoil particles from Po^{210} and their ionization in argon and helium. *Phys. Rev.* **1956**, *102*, 389–390. [CrossRef]
29. Cano, G.L. Total ionization and range of low-energy recoil particles in pure and binary gases. *Phys. Rev.* **1968**, *169*, 277–280. [CrossRef]
30. Ling, R.C.; Knipp, J.K. Ionization by recoil particles from alpha-decay. *Phys. Rev.* **1950**, *80*, 106. [CrossRef]
31. Watanabe, T.; Katsuura, K. Ionization of atoms by collision with excited atoms. II. A formula without the rotating-atom approximation. *J. Chem. Phys.* **1967**, *47*, 800. [CrossRef]
32. Dexter, D.L. A Theory of sensitized luminescence in solids. *J. Chem. Phys.* **1953**, *21*, 836–850. [CrossRef]
33. SRIM2013. Available online: http://www.srim.org/ (accessed on 6 October 2020).
34. Hitachi, A.; Mozumder, A. Properties for liquid argon scintillation for dark matter searches. *arXiv* **2019**, arXiv:1903.05815.
35. Xu, J.; Stanford, C.; Westerdale, S.; Calaprice, F.; Wright, A.; Shi, Z. First measurement of surface nuclear recoil background for argon dark matter searches. *Phys. Rev. D* **2017**, *96*, 061101(R). [CrossRef]
36. Cao, H.; Alexander, T.; Aprahamian, A.; Avetisyan, R.; Back, H.O.; Cocco, A.G.; DeJongh, F.; Fiorillo, G.; Galbiati, C.; Guardincerri, Y.; et al. (SCENE collaboration). Measurement of scintillation and ionization yield and scintillation pulse shape from nuclear recoils in liquid argon. *Phys. Rev. D* **2015**, *91*, 092007. [CrossRef]
37. Galbiati, C. (WARP Collaboration). First Physics Results from WARP 2.3 Liter Prototype. Available online: http://cosmology.berkeley.edu/inpac/CDMSCE_Jun06/Talks/WARP%20SUSY06.pdf (accessed on 24 November 2020).
38. Tanaka, M.; Doke, T.; Hitachi, A.; Kato, T.; Kikuchi, J.; Masuda, K.; Murakami, T.; Nishikido, F.; Okada, H.; Ozaki, K.; et al. LET dependence of scintillation yields in liquid xenon. *Nucl. Instrum. Methods Phys. Res. Sect. A Accel. Spectrometers Detect. Assoc. Equip.* **2001**, *457*, 454–463. [CrossRef]
39. Dahl, C.E. The Physics of Background Discrimination in Liquid Xenon, and First Results from XENON10 in the Hunt for WIMP Dark Matter. Ph. D. Thesis, Princeton University, Princeton, NJ, USA, 2009.
40. Murray, R.B.; Mayer, A. Scintillation response of activated ionic crystals to various charged particles. *Phy. Rev.* **1961**, *122*, 815–826. [CrossRef]
41. Doke, T.; Shibamura, E.; Kubota, S. Maximum scintillation yield in NaI(Tl). *J. Phys. Soc. Jpn.* **1999**, *68*, 2433–2438. [CrossRef]
42. Yunoki, A.; Doke, T.; Fukuda, N.; Kase, M.; Kato, T.; Kikuchi, J.; Masuda, K.; Niimura, M.; Okada, H.; Ozaki, K.; et al. An allene-doped liquid argon ionization chamber for Ar and Ca ions at around 100 MeV/n. *Nucl. Instrum. Methods Phys. Res. Sect. A* **1999**, *432*, 332–341. [CrossRef]
43. Anderson, D.F. The effects of photosensitive dopants on electron mobility in liquid argon. *Nucl. Instr. Meth. A* **1992**, *313*, 151–154. [CrossRef]
44. Hitachi, A.; Ichinose, H.; Doke, T.; Shibamura, E.; Kikuchi, J.; Masuda, K. Photoionization quantum yields of organic molecules in liquid argon and xenon. *Phys. Rev. B* **1997**, *55*, 5742–5748. [CrossRef]
45. Mu, W.; Xiong, X.; Ji, X. Scintillation efficiency for low energy nuclear recoils in liquid xenon dark matter detectors. *Astropart. Phys.* **2015**, *61*, 56–61. [CrossRef]
46. Barker, D.; Mei, D.-M. Germanium detector response to nuclear recoils in search for dark matter. *Astrop. Phys.* **2012**, *38*, 1–6. [CrossRef]
47. Lindhard, J.; Sharff, M.; Schiøtt, H.E. Range concepts and heavy ion ranges. *Mat. Fys. Medd. Dan. Vid. Selsk.* **1963**, *33*, 1–42.
48. Fano, U.; Lichten, W. Interpretation of Ar+-Ar collisions at 50 KeV. *Phys. Rev. Lett.* **1965**, *14*, 627–629. [CrossRef]
49. Garcia, J.D.; Fortner, R.J.; Kavanagh, T.M. Inner-shell vacancy production in ion-atom collisions. *Rev. Mod. Phys.* **1973**, *45*, 111–177. [CrossRef]
50. Guillaudin, O.; Billard, J.; Bosson, G.; Bourrion, O.; Lamy, T.; Mayet, F.; Santos, D.; Sortais, P. Quenching factor measurement in low pressure gas detector for directional dark matter search. In Proceedings of the Sygnus 2011: Third International Conference on Directional Detection of Dark Matter, Aussois, France, 7–10 June 2011; Fayet, F., Santos, D., Eds.; 2012; 53, pp. 119–127. [CrossRef]
51. Bolotnikov, A.; Ramsey, B. The spectroscopic properties of high-pressure xenon. *Nucl. Instrum. Methods Phys. Res. Sect. A* **1997**, *396*, 360–370. [CrossRef]
52. Kusano, H.; Ishikawa, T.; Lopes, J.A.; Miyajima, M.; Shibamura, E.; Hasebe, N. Scintillation and ionization yields produced by α-particles in high density gaseous xenon. *Nucl. Instrum. Methods Phys. Res. Sect. A* **2012**, *683*, 40–45. [CrossRef]
53. Lopes, M.I.; Chepel, V. Rare gas liquid detectors. In *Electronic Excitations in Liquified Rare Gases*; Schmidt, W.F., Illenberger, E., Eds.; American Scientific Publishers: Portland, OR, USA, 2005; Chapter 11; pp. 331–338.

54. Hitachi, A.; LaVerne, J.A.; Doke, T. Effect of an electric field on luminescence quenching in liquid argon. *Phys. Rev. B* **1992**, *46*, 540–543. [CrossRef]
55. Salamon, M.H.; Ahlen, S.P. NaI:Tl response to relativistic Ne, Ar, and Fe ions. *Phys. Rev. B* **1981**, *24*, 5026–5036. [CrossRef]
56. Collar, J.I.; Kavner, A.R.L.; Lewis, C.M. Response of CsI(Na) to nuclear recoils; Impact on coherent elastic neutrino-nucleus scattering (CEνNS). *Phys. Rev. D*. **2019**, *100*, 033003. [CrossRef]